J Mater Sci: Mater Electron (2020) 31:17474–17481

Study of the optical and gas sensing properties of In_2O_3 nanoparticles synthesized by rapid sonochemical method

Hafeez Ullah[1,*], Zain H. Yamani[2], Ahsanulhaq Qurashi[2,5], Javed Iqbal[3], and Kashif Safeen[4]

[1] *Institute of Physics & Electronics, Gomal University, Dera Ismail Khan 29220, KP, Pakistan*
[2] *Center of Excellence in Nanotechnology (CENT), KFUPM, Dhahran 31261, Saudi Arabia*
[3] *Laboratory of Nanoscience and Technology (LNT), Department of Physics, Quaid-I-Azam University Islamabad, Islamabad, Pakistan*
[4] *Department of Physics, Abdul Wali Khan University Mardan, Mardan, Pakistan*
[5] *Department of Chemistry, Khalifa University, Abu Dhabi 127788, United Arab Emirates*

Received: 25 February 2020
Accepted: 19 August 2020
Published online:
31 August 2020

ABSTRACT

Indium oxide (In_2O_3) nanoparticles were synthesized via a facile rapid sonochemical method. Detailed spectroscopic techniques were used to investigate optical, structural and chemical properties of the synthesized In_2O_3 nanoparticles. The structural analysis shows that In_2O_3 nanoparticles have cubic structure and are polycrystalline in nature. The morphology of the In_2O_3 nanoparticles examined by field emission scanning electron microscopy revealed spherical and uniformly distributed particles. Bruno emit Teller surface analyzer demonstrated that the surface areas of In_2O_3 nanoparticles is 45 m^2/g and also confirmed that the synthesized nanoparticles are mesoporous. Raman spectra also revealed that the synthesized nanoparticles have cubic structure. In–O band stretching of the synthesized In_2O_3 nanoparticles was confirmed using Fourier Transform Infrared Spectroscopy. Photoluminescence spectra of the In_2O_3 nanoparticles showed broad and intense UV emission peak at 358 nm. Moreover, the synthesized In_2O_3 nanoparticles showed good sensitivity and fast response toward the hydrogen gas at lower temperature.

1 Introduction

Nanostructure semiconducting materials demonstrate very interesting chemical, optical properties compared to those of bulk materials. These nanostructures semiconductor materials exhibit extraordinary properties towards the novel devices [1]. In last decade, various type of nanostructures were synthesized to optimize different kinds of properties such as chemical, electrical and optical

Address correspondence to E-mail: hafeezullah83@gmial.com

https://doi.org/10.1007/s10854-020-04303-9

properties of these nanostructure materials. In_2O_3 has a wide band gap (3.6 eV) n-type semiconductor having large applications in many fields including solar cell, gas sensor, field emission display, biosensor, optoelectronics and photo catalysis [2–8]. Various chemical and physical vapor deposition techniques including sol gel, co precipitation, pulse laser depositions, thermal evaporation and sputtering have been used for the preparation of Indium oxide nanostructure. However, these techniques involved complicated procedure, deployed expansive equipments and required high energy for operation. On the other hand, wet chemistry method used in the present work required low energy, economical and is easy to handle. The wet chemistry method includes spray pyrolysis, spin- and dip-coating [9]. Furthermore, the indium oxide nanostructure materials have been synthesized using the surfactant templates method. However, the sol–gel method and co-precipitation method are the mostly used method for synthesis of these nanoparticles. Using the wet chemistry approach, the surface morphology, shape, crystallinity and particles size of indium oxide nanoparticles can be controlled. Further, highly crystalline nanoparticles can be obtained using the wet chemistry approach at moderate temperature. Amongst wet chemistry synthesis approach, recently sonochemistry has been attracted great attention for the synthesis of ultrafine metal oxide nanostructure. In this technique, the cavitation and microbubbles are generated with powerful ultrasound radiation. Parameters of the process can be controlled easily in the sonochemical method. The important parameters of the sonochemical reaction are the bob vibrating frequencies, temperature plays significant role in the size of the particles, shape morphology and the crystallinity of indium oxide nanoparticles [10–12].

In this paper, In_2O_3 nanoparticles were synthesized by simplest sonochemical method for the gas sensor applications. The synthesized In_2O_3 nanoparticles were characterized using various techniques demonstrated well excited optical properties, structural and shows good response toward the hydrogen gas. Moreover, the synthesized In_2O_3 nanoparticles can be used in high conducting transparent oxide in other optoelectronics devices.

2 Experimental

In_2O_3 nanoparticles were synthesized using indium acetylacetonate (high purity Sigma–Aldrich) as a precursor. The appropriate quantity of indium acetylacetonate precursors were dissolved in the distilled water. 4 mL NH_4OH was added to the prepare solvent in order to maintain pH around 9–10 during the sonochemical process. The obtained yields in the solution form have been treated using a high ultrasonic intensity processor (Power = 750 W, frequency = 20 kHz and Ti-probe tip = 6 mm) via direct-immersion way for 60 min. During the sonication's the temperature of the precursor's solution was fixed in the range of 80–90 °C using a water bath. After the sonication the homogeneous and transparent solution were obtained. In order to removal the acetate and other residues, the final solutions have been centrifuged and subsequently washed numerous times using deionized water. The obtained powders were at 70 °C in the oven. Finally, the dried powders were calcined at different temperatures 400 °C, 700 °C, and 800 °C for 2 h.

The crystalline phase and crystallite size of the synthesized In_2O_3nanoparticles was investigated using Mini-X-ray Diffraction (Mini-XRD) with CuKα X-ray radiation (λ = 0.15406 nm). The morphology, size of In_2O_3nanoparticles and chemical composition has been examined with (FESEM/FIB/GIS (Tescan Lyra-3) and EDX equipped with FESEM. The surface area and porosity of In_2O_3 nanoparticles were carried out by surface area and porosity analyzer (ASAP2020). The photoluminance spectrum of the In_2O_3 nanoparticles were measured at room temperature by the fluorescence spectrometer (FLS920) using Xe lamp with excitation wavelength λ_{ex} = 315 nm. The Raman spectrum was taken at room temperature with IHR320 Horiba Spectrometer with CCD.

3 Results and discussion

3.1 XRD analysis

Figure 1 shows the XRD patterns of In_2O_3 nanoparticles calcined at 400 °C. In the XRD spectrum peak positions at 21.39, 30.89, 35.59, 51.45, and 60.72 are assigned to reflections of the planes (211), (222), (400), (440) and (622), respectively. The highest intensity of the (222) diffraction peak clearly shows that the prepared In_2O_3 nanoparticles are cubic polycrystalline structure. The peak position in the XRD pattern shows the cubic structure by comparing with standard pattern of cubic structure of In_2O_3 (JCPDS No. 06-0416). The lattice parameter and cell volume of the In_2O_3 nanoparticles is calculated using the following equations.

$$a = d_{hkl}(l^2 + h^2 + k^2)^{1/2} \quad (1)$$

$$V = a^3 \quad (2)$$

where "a" is the lattice parameter, h, k and l are the miller indices of the plane and d_{hkl} is the inter-planar spacing. The experimentally obtained lattice parameter "a" and cell volume "V" of the In_2O_3 nanoparticles are 10.07 Å and 1021.14 Å^3 respectively.

The crystallite size of the In_2O_3 nanoparticles determined using the Williamson–Hall plot of βcosθ along axis and put 4sinθ y axis, using Eq. (2) was applied to the (222), (400), and (440) peaks. The plot of 4sinθ versus βcosθ taking (222), (400), and (440) lattice planes. The crystallite size D was extracted from the linear fit from the intercept at y-axis.

$$\beta_{\mathrm{hkl}} \cos\theta = \frac{K\lambda}{D} + 4\varepsilon \sin\theta \quad (3)$$

Here β_{hkl} is the full width at half-maximum (FWHM) of the peak considered (in rad) corresponding to be induced by both the average crystallite size D and strain ε. Where λ is the X-ray wavelength (0.1541 nm) for CuKα radiation while K is approximately equal to 0.9. The crystallite sizes and strain of the In_2O_3 nanoparticles are15.2 ± 1.8 nm and 6.5 × 10^{-3} respectively.

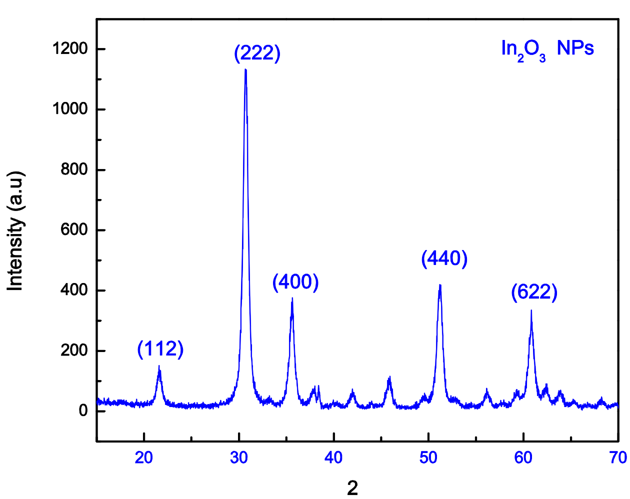

Fig. 1 XRD pattern of indium oxide nanoparticles calcined at 400 °C

3.2 SEM and EDX analysis

Figure 2a, b shows the morphology of In_2O_3 nanoparticles taken at resolution of 1 µm and 500 nm, respectively. FESEM images indicate that the synthesized In_2O_3nanoparticles are in spherical shape and homogeneously spread. The FESEM micrographs are also demonstrated that the synthesized In_2O_3 nanoparticles size in the range from 15 to 30 nm and well disperse. The sizes of the In_2O_3 nanoparticles from the FESEM micrograph are good agreement with XRD finding.

The energy-dispersive spectroscopy has been used for the chemical and compositional analysis of In_2O_3 nanoparticles. Figure 3 shows the EDX spectrum that the presence of oxygen and indium elements. An extra peak also appeared in the EDX spectrum which might be associated with gold induced from coating of the sample for analysis.

3.3 Photoluminescence properties

Figure 4 shows the room temperature PL spectra of In_2O_3 nanoparticles, measured by means of Xenon laser of wave length 250 nm used as excitation source. The strong UV emission of the In_2O_3 nanoparticles have been obtained at broad band centered at ~ 358 nm (3.47 eV). Such kind of emission is not reported for bulk In_2O_3 [13]. In the present case, it can be linked with the nanostructure In_2O_3 as validated from the FESEM and XRD analysis. One possibility of this emission could be oxygen vacancies as reported in literature [14–17]. The arises of oxygen vacancies in the synthesized In_2O_3 nanoparticles can be explained as follow, during calcination of the In_2O_3 nanoparticles, some sight of oxygen become incomplete or might be some intrinsic defects arises, which could be related to the oxygen vacancies [17]. The suppression of defect-related emission of In_2O_3 is correlated to the reconstruction of defect structures. These oxygen vacancies formed new energy level near or in the band gap of the $In_2O_3,$ which could be normally acted as deep defects donors' level. The strong UV emission of the In_2O_3 nanoparticles might be the radiative recombination of the photo-excited holes and electrons occupied by oxygen vacancies. Similar mechanism is already explained for the ZnO

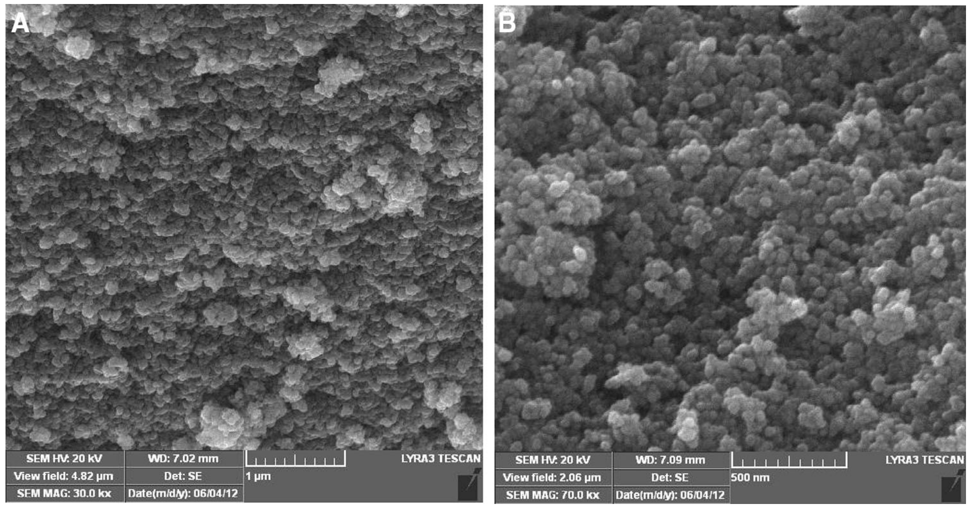

Fig. 2 **a** FESEM image of In_2O_3 nanoparticles taken at resolution of 1 μm. **b** FESEM image of In_2O_3 nanoparticles taken at resolution of 500 nm

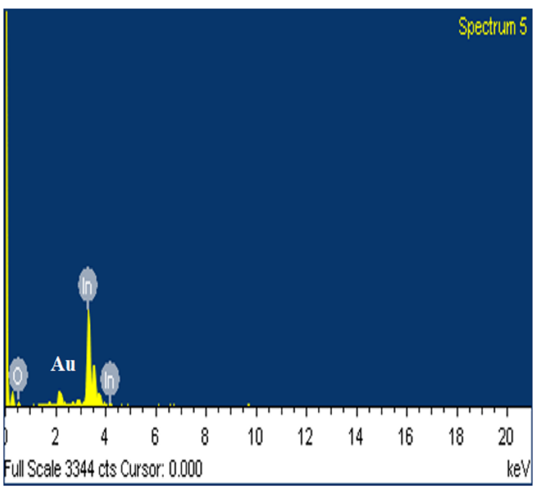

Fig. 3 EDX spectrum of In_2O_3 nanoparticles

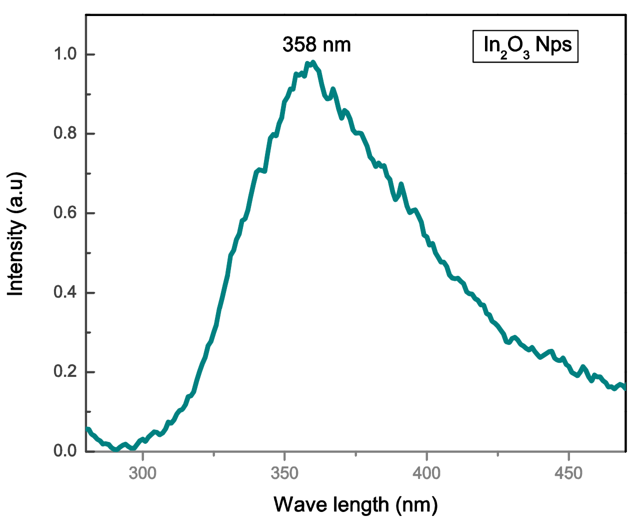

Fig. 4 Photoluminescence of In_2O_3 nanoparticles

and SnO_2 semiconductor [18]. The other possibilities of the oxygen vacancies could the size of the indium oxide nanoparticles. It is already mentioned in the FESEM analysis that the synthesized In_2O_3 nanoparticles size is in the range of 15–30 nm. The small size would favor the existence of oxygen vacancies for the high surface to volume ratio of In_2O_3 nanowires [19].

3.4 Brunauer–Emmett–Teller

Brunauer–Emmett–Teller (BET) method was employed to determine the specific surface area and pore size of the In_2O_3 nanoparticles in the N_2 adsorption–desorption isotherm. Figure 5 illustrates the isotherm of In_2O_3 nanoparticles. The synthesized In_2O_3 nanoparticles are related to the type IV profile of the adsorption–desorption isotherm indicating the mesoporous nature of the nanoparticles. The estimated surface area, pore size and volume of the synthesized In_2O_3 nanoparticles were found around of 45 m^2/g, 10.5 nm and 0.28 cm^3/g, respectively.

3.5 FTIR spectra

Room temperature FTIR spectra of In_2O_3 were recorded (range 400–4000 cm^{-1}) to confirm the stretching vibration of In–O bonds (see Fig. 6). The spectra contain high adsorption stretching. The stretching band near to 1990 cm^{-1}arises due to C–H stretching confirmed [20]. The nitrate group band stretching and bends deformation of water appeared at 1630 cm^{-1} [21]. The presence of high intensity stretching vibration band of OH and C–H might be the adsorption of the moister from the surrounding

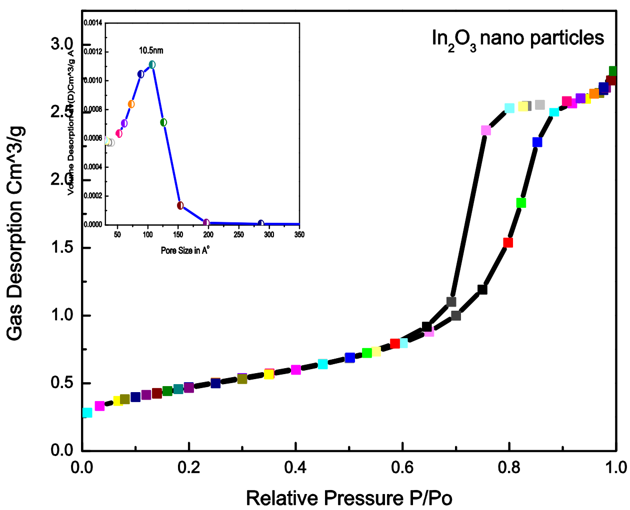

Fig. 5 Nitrogen adsorption–desorption isotherms of In_2O_3 nanoparticles

after the calcination of the synthesized samples. The In–O band stretching is appeared at about 630 cm^{-1}. Concluding the FTIR analysis, it is clearly confirmed that the synthesized indium oxide has In–O band stretching at about 630 cm^{-1}.

3.6 Raman spectroscopy

Raman spectroscopy were used to identify the low energy modes of In_2O_3 nanoparticles, the disorderness induce in the modes due to the strain after the calcination of the synthesized In_2O_3 nanoparticles. Cubic In_2O_3 belongs to $I^3{}_a$ and $T^1{}_h$ space group. For the cubic In_2O_3, the total expected low energy active Raman mode in the infrared region were 22 and 16. Wang et al. and Zhang et al. reported 6 Raman modes and 11 infrared modes for cubic In_2O_3 [22, 23]. The Raman mode which is always active in vibration symmetry are A_g, E_g, T_g and T_u [22, 24]. Figure 7 shows the Raman spectrum of the prepared samples calcinated at 400 °C, 600 °C and 800 °C. Five vibrational modes were observed in the Raman spectra calcined at 600 °C, which appeared at 303 cm^{-1}, 364 cm^{-1},435 cm^{-1}, 492 cm^{-1} and 619 cm^{-1}. From the literature, these modes are belonging to In_2O_3 cubic structure [25]. The shift in Raman peaks towards the lower wave numbers observed with increasing the calcination temperature. This shift may be due to the presence of defects as function of calcination temperature such as strain and other structural defects induced in the structure of In_2O_3 with the increasing calcination temperature. Structural disordering in the Raman spectroscopy is mainly due to defects induced in the metal oxide structure which may be caused to break the selection rule.

3.7 Gas sensing properties

Figure 8 shows the measurement setup for gas sensing properties of In_2O_3 nanoparticles. The gas sensing response of the samples was investigated with variation of time versus the electrical resistance for ambient of hydrogen gas. The response time, defined as the time needs to drop the resistance of the sensing material by 90% of the initial baseline resistance with

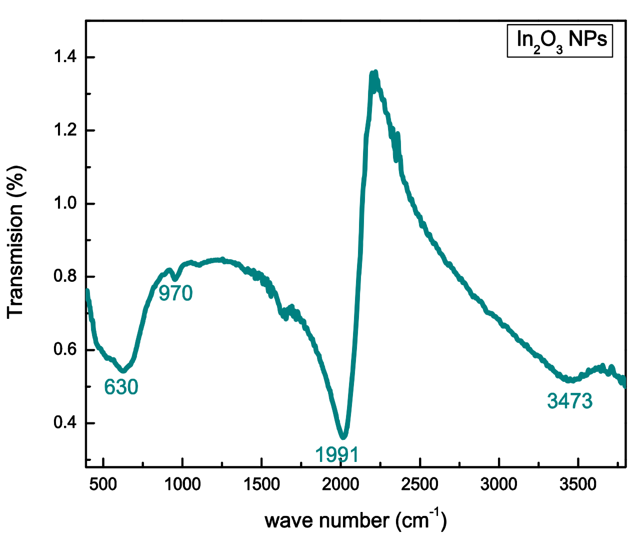

Fig. 6 The FTIR spectra of In_2O_3 nanoparticles

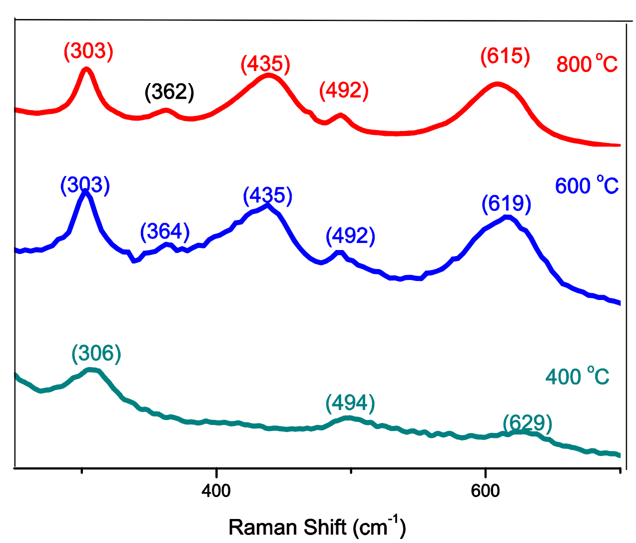

Fig. 7 Raman spectra of In_2O_3 nanoparticles calcined at 400 °C, 600 °C and 800 °C

introducing of the H_2 gas to the sensing material. The response time is important characteristic of the sensor after changing the gas ambient. The response time of the In_2O_3nanoparticles and the changing the ambient gas of these nanoparticles are illustrated in Fig. 9.

Figure 9 presents the gas sensing properties of In_2O_3 nanoparticles for hydrogen (H_2) gas. Very quick response toward the hydrogen gas was observed by In_2O_3 nanoparticles at 200 °C. Correspondingly, the sensor returns again very quickly to its original position after purging out the H_2 gas. The quick and fast response of the In_2O_3 nanoparticle toward the H_2 gas could be full surface area exposure of the In_2O_3 molecules to the chemical environment.

As from the BET measurement is demonstrated that the In_2O_3 nanoparticles have large surface area to volume. Due to this large surface area of the In_2O_3 nanoparticles, a greater number of In_2O_3 molecules are available to contribute the surface reaction. It is well known that as the size of particles decreases, the surface area is increased vice versa. The behavior of the response of the In_2O_3 nanoparticles is related to the surface reaction of the oxygen species and the reducing gas in contact [26–28]. Increasing surface area of In_2O_3 nanoparticles increases adsorption sites and hence large number *of* oxygen species is available for the reaction. Significant change in the resistance due the interaction of reducing gas shows higher sensitivity of the sensor [29]. This feature can contribute to the change in the resistance of In_2O_3 nanoparticles, with enhance sensing response and lower working temperature. Moreover, for

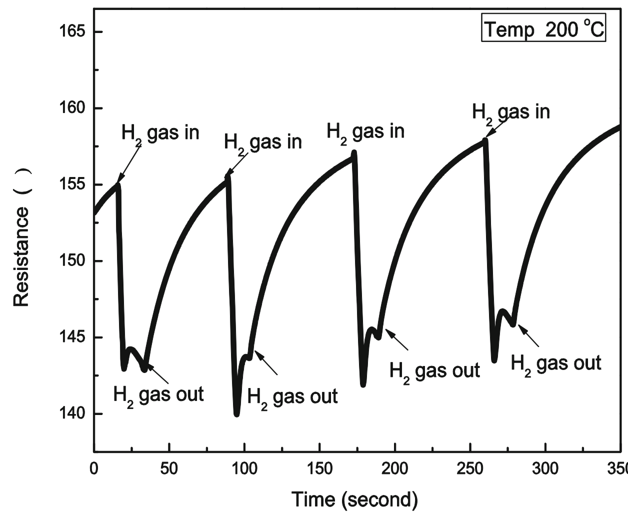

Fig. 9 Gas sensing properties of In_2O_3 nanoparticles at 200 °C

improving the sensor sensitivity, particle size and porosity of the prepared material structure must be taken into consideration, which depends upon the sensor surface area [30]. The sensitivity of the gas response of In_2O_3 semiconductor can be measured through the power-law relation [31].

$$S(\%) = \frac{R_{air} - R_{hydrogen}}{R_{air}} \times 100 \quad (4)$$

The sensitivity can be calculated from the power law. The sensitivity of the of In_2O_3 nanoparticles was around 13.5% ± 1%. The response time estimated was around 30 to 35 s while the recovery time was found 40 to 45 s. When H_2 gas reacts with In_2O_3 nanoparticles, it has been found that the baseline

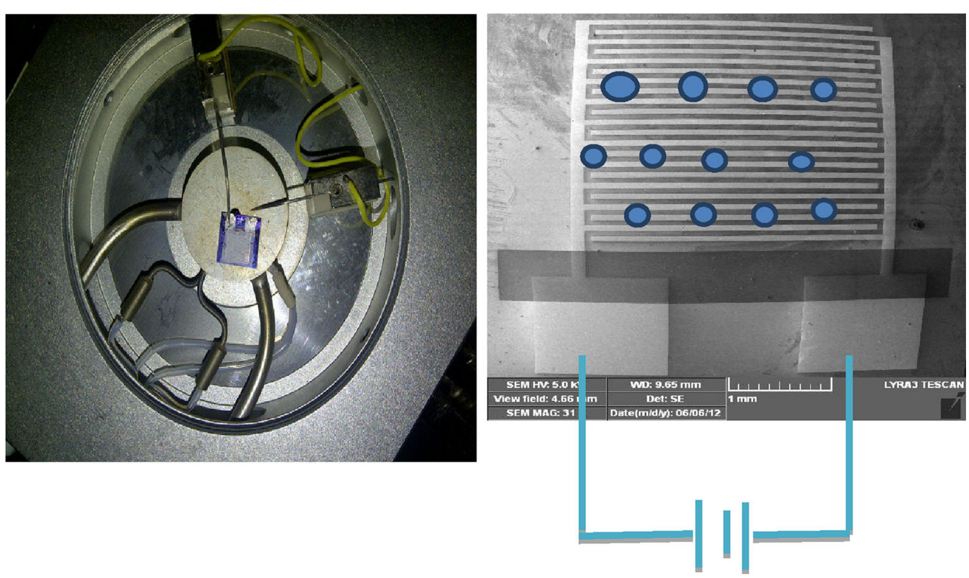

Fig. 8 Measurement setup for gas sensing properties of In_2O_3 nanoparticles

resistance of the In_2O_3 nanoparticles is much low (in the range of 50–250 Ω). It has been established that low resistance of the sensing material layer is very suitable for the reduction of the noise in the analysis and consequently shows the high signal/noise ratio. The decrease in the resistance of In_2O_3 in H_2 gas sensing might be the n-type semiconducting behavior of these nanoparticle also having high mobility and more intrinsic electronic concentrations [32].

4 Conclusion

The In_2O_3 nanoparticles were successfully prepared using sonochemical techniques. The X-ray diffraction result demonstrated that the synthesized In_2O_3 nanoparticles have crystallite nature with cubic structure. The crystallite size and strain of the In_2O_3nanoparticles estimated from XRD were 15.2 ± 1.8 nm and 6.5 × 10^{-3}. FESEM micrographs show that In_2O_3 nanoparticles have spherical and uniformly distributed particles. EDX spectrum confirmed the presence of indium and oxygen elements. The photoluminescence spectra of the In_2O_3 nanoparticles showed broad and intense UV emission peak at 358 nm (3.47 eV). The Raman active modes at 629 cm^{-1} (E_{2g}), 494 cm^{-1} (A_{1g}), 306 cm^{-1} (E_{1g}) of the calcined sample at 400 °C confirmed the cubic structure of In_2O_3. BET of the nanoparticles shows that the N_2 adsorption–desorption has isotherm of type IV. The BET specific area of the In_2O_3 nanoparticles is 45 m^2/g. FTIR results confirm nature of molecular bonding in In_2O_3. The gas sensitivity of In_2O_3 nanoparticles measured at 200 °C showed good response for hydrogen gas. This would contribute to the safe development of hydrogen energy for various applications.

Acknowledgements

The support of this work has been provided by King Abdul-Aziz City for Science and Technology (KACST). The funding for this work has been came through project 09-NAN772-04, which is a as part of the National Science, Technology and Innovation Plan and all the synthesis and characterizations of the prepared sample has been carried out in the Centre of excellence and Nanotechnology (CENT) & KFUPM.

References

1. Z.B. Zhou, R.Q. Cui, Q.J. Pang, Y.D. Wang, F.Y. Meng, T.T. Sun, Z.M. Ding, X.B. Yu, Preparation of indium tin oxide films and doped tin oxide films by an ultrasonic spray CVD process. Appl. Surf. Sci. **172**(3–4), 245–252 (2001)
2. Y.X. Liang, S.Q. Li, L. Nie, Y.G. Wang, T.H. Wang, In situ synthesis of In_2O_3 nanowires with different diameters from indium film. Appl. Phys. Lett. **88**(19), 193119 (2006)
3. D.W. Kim, I.S. Hwang, S.J. Kwon, H.Y. Kang, K.S. Park, Y.J. Choi, K.J. Choi, J.G. Park, Highly conductive coaxial $SnO_2-In_2O_3$heterostructured nanowires for Li ion battery electrodes. Nano Lett. **7**(10), 3041–3045 (2007)
4. M. Curreli, C. Li, Y. Sun, B. Lei, M.A. Gunderson, M.E. Thompson, C. Zhou, Selective functionalization of In_2O_3 nanowire mat devices for bio sensing applications. J. Am. Chem. Soc. **127**(19), 6922–6923 (2005)
5. S. Bianchi, E. Comini, M. Ferroni, G. Faglia, A. Vomiero, G. Sberveglieri, Indium oxide quasi-monodimensional low temperature gas sensor. Sens. Actuators B Chem. **118**(1–2), 204–207 (2006)
6. C.Y. Kuo, S.Y. Lu, T.Y. Wei, In_2O_3 nanorod formation induced by substrate structure. J. Cryst. Growth **285**(3), 400–407 (2005)
7. B. Li, Y. Xie, M. Jing, G. Rong, Y. Tang, G. Zhang, In_2O_3 hollow microspheres: synthesis from designed $In(OH)_3$ precursors and applications in gas sensors and photocatalysis. Langmuir **22**(22), 9380–9385 (2006)
8. A. Gurlo, M. Ivanovskaya, N. Barsan, M. Schweizer-Berberich, U. Weimar, W. Göpel, A. Dieguez, Grain size control in Nano crystalline In_2O_3 semiconductor gas sensors. Sens. Actuators B Chem. **44**(1–3), 327–333 (1997)
9. C. Goebbert, H. Bisht, N. Al-Dahoudi, R. Nonninger, M.A. Aegerter, H. Schmidt, Wet chemical deposition of crystalline, redispersable ATO and ITO nanoparticles. J. Sol–Gel Sci. Technol. **19**(1–3), 201–204 (2000)
10. K.S. Suslick, S.-B. Choe, A.A. Cichowlas, M.W. Grinsta, Sonochemical synthesis of amorphous iron. Nature **353**, 414–416 (1991)
11. K.S. Suslick, Sonochemistry. Science **247**(4949), 1439–1445 (1990)
12. H. Frenzel, H. Schultes, Experimental investigation of acoustic cavitation in gaseous liquids. Z. Phys. Chem. **27**, 421–424 (1934)
13. M. Epifani, R. Díaz, J. Arbiol, P. Siciliano, J.R. Morante, Solution synthesis of thin films in the $SnO_2-In_2O_3$ system: a case study of the mixing of sol−gel and metal-organic solution processes. Chem. Mater. **18**(3), 840–884 (2006)

14. M.J. Alam, D.C. Cameron, Investigation of annealing effects on sol–gel deposited indium tin oxide thin films in different atmospheres. Thin Solid Films **420**, 76–82 (2002)
15. C. Goebbert, R. Nonninger, M.A. Aegerter, H. Schmidt, Wet chemical deposition of ATO and ITO coatings using crystalline nanoparticles redispersable in solutions. Thin Solid Films **351**(1–2), 79–84 (1999)
16. J. Ederth, P. Johnsson, G.A. Niklasson, A. Hoel, A. Hultaker, P. Heszler, C.G. Granqvist, A.R.V. Doorn, M.J. Jongerius, D. Burgard, Phys. Rev. B **68**, 410 (2003)
17. N. Al-Dahoudi, M.A. Aegerter, Wet coating deposition of ITO coatings on plastic substrates. J. Sol–Gel. Sci. Technol. **26**(1–3), 693–697 (2003)
18. S.M. Kim, K.H. Seo, J.H. Lee, J.J. Kim, H.Y. Lee, J.S. Lee, Preparation and sintering of nanocrystalline ITO powders with different SnO_2 content. J. Eur. Ceram. Soc. **26**(1–2), 73–80 (2006)
19. H.R. Xu, G.S. Zhu, H.Y. Zhou, A.B. Yu, Preparation of monodispersed tin-doped indium oxide nanopowders under moderate conditions. Mater. Lett. **59**(1), 19–21 (2005)
20. J. Chandradass, K.-S. Han, D.S. Bae, J. Mater. Sci. Technol. **206**, 315 (2008)
21. V.N. Singh, B.R. Mehta, R.K. Joshi, F.E. Kruis, S.M. Shivaprasad, Enhanced gas sensing properties of In_2O_3: Ag composite nanoparticle layers; electronic interaction, size and surface induced effects. Sens. Actuators B Chem. **125**(2), 482–488 (2007)
22. C.Y. Wang, Y. Dai, J. Pezoldt, B. Lu, T. Kups, V. Cimalla, O. Ambacher, Phase stabilization and phonon properties of single crystalline rhombohedral indium oxide. Cryst. Growth Des. **8**(4), 1257–1260 (2008)
23. S.B. Zhang, S.H. Wei, A. Zunger, H. Katayama-Yoshida, Defect physics of the $CuInSe_2$ chalcopyrite semiconductor. Phys. Rev. B **57**(16), 9642 (1998)
24. M. Kumar, V.N. Singh, F. Singh, K.V. Lakshmi, B.R. Mehta, J.P. Singh, On the origin of photoluminescence in indium oxide octahedron structures. Appl. Phys. Lett. **92**(17), 171907 (2008)
25. A.J.C. Lanfredi, R. Geraldes, O.M. Berengue, W.R. Leite, A.J. Chiquito, J. Appl. Phys. **105**, 23708 (2009)
26. G. Gaggiotti, A. Galdikas, S. Kaciulis, G. Mattogno, A. Setkus, Temperature dependencies of sensitivity and surface chemical composition of SnOx gas sensors. Sens. Actuators B Chem. **25**(1–3), 516–519 (1995)
27. W.Y. Chung, T.H. Kim, Y.H. Hong, D.D. Lee, Characterization of porous tin oxide thin films and their application to microsensor fabrication. Sens. Actuators B Chem. **25**(1–3), 482–485 (1995)
28. K. Daoudi, C.S. Sandu, A. Moadhen, C. Ghica, B. Canut, V.S. Teodorescu, M.G. Blanchin, J.A. Roger, M. Oueslati, B.Bessais, ITO spin-coated porous silicon structures. Mater. Sci. Eng. B **101**(1–3), 262–265 (2003)
29. G.J. Li, X.H. Zhang, S. Kawi, Relationships between sensitivity, catalytic activity, and surface areas of SnO_2 gas sensors. Sens. Actuators B Chem. **60**(1), 64–70 (1999)
30. G.J. Li, S. Kawi, High-surface-area SnO_2: a novel semiconductor-oxide gas sensor. Mater. Lett. **34**(1–2), 99–102 (1998)
31. H. Dong, Z. Li, Z. Ding, H. Pan, X. Wang, X. Fu, Nanoplates of α-$SnWO_4$ and SnW_3O_9 prepared via a facile hydrothermal method and their gas-sensing property. Sens. Actuators B Chem. **140**(2), 623–628 (2009)
32. M.H. Seo, M. Yuasa, T. Kida, J.S. Huh, K. Shimanoe, N. Yamazoe, Gas sensing characteristics and porosity control of nanostructured films composed of TiO_2 nanotubes. Sens. Actuators B Chem. **137**(2), 513–520 (2009)